Life cycle of deep convective systems over the eastern tropical Pacific observed by TRMM and GOES-W

Toshiro Inoue[1,2] , Daniel Vila[3], Kavirajan Rajendran[4], Atsushi Hamada[5], Xiangqian Wu[6] and Luiz Machado[7]

1) Center for Climate System Research, Kashiwa, Japan

2) Meteorological Research Institute, Tsukuba, Japan

3) University of Maryland, USA

4) CSIR-Center for Mathematical Modeling and Computer Simulation, National Aerospace Laboratories, Bangalore, India

5) Kyoto University, Kyoto, Japan

6) Center for Satellite Applications and Research/NOAA, USA

7) CPTEC/INPE, Cachoeira Paulista, Brazil

13 June 2008, Submitted to Special Issue of JMSJ

12 January 2009, Final Revision

Corresponding author address: Toshiro Inoue, toshiro@ccsr.u-tokyo.ac.jp

Center for Climate System Research, The University of Tokyo, 5-1-5 Kashiwanoha, Kashiwa-shi, Chiba, 277-8568, Japan

Abstract

The life cycle of deep convective systems over the eastern tropical Pacific (30N to 30S, 180 to 90W) was studied in terms of cloud types, as classified by a split window (11 μm and 12 μm). Hourly split window image data of Geostationary Operational Environmental Satellite (GOES-W) from January 2001 to December 2002 was used in this study. Deep convection consists mostly of optically thick cumulus type clouds in the earlier stage and a cirrus type cloud area that increases with time in the later stage. During this analysis period and over the analysis area, the life stage of deep convection, to a large extent, can be identified by computing the percentage of cirrus type clouds within the deep convection from a single snap shot of the split window image. Coincident Tropical Rainfall Measuring Mission (TRMM) Precipitation Radar (PR) observations were used to study the relationship between the percentage of cirrus type clouds within a deep convection (i.e., its life stage) and the rainfall rate from TRMM PR. It was found that the rainfall rate tends to be larger in the earlier stage of the life cycle when a smaller percentage of cirrus type cloud is present within the deep convection.

1. Introduction

Deep convective systems (DC) are significant meteorological phenomena, since severe thunderstorms are often associated with them. Advancing our knowledge of how DC originate, mature and decay is a fundamental issue in atmospheric science. A pioneering study by Byers and Braham (1949) demonstrated the life cycle of a DC using aircraft and radar observations. They summarized the life cycle of a DC as comprising a developing stage, a mature stage and a dissipating stage. The dominant cloud types at the three stages are cumulus, cumulonimbus and anvil clouds. They also suggested that the rainfall type differed depending on the life stage. Thus, to identify the life stage of a DC from a single satellite image provides us with important information on the DC.

Satellite observations from a geostationary orbit are useful in studying the evolution of DCs, considering the high number of temporal observations and wide range of coverage. Many studies have been conducted to study DCs using infrared and/or visible radiance images from geostationary weather satellites (e.g., Murakami, 1983; Williams and Houze, 1987; Nakazawa,1988; Duvel, 1989; Takayabu, 1994). These studies mostly used single infrared data to delineate DCs by determining the threshold of brightness the temperature in the infrared channel (TBB).

Mapes and Houze (1993) studied cloud clusters over a warm pool in the western Pacific using an improved the objective cloud-cluster tracking technique developed by Williams and Houze (1987). They used a TBB threshold of -65 C to identify a cloud cluster and showed the early morning maximum of the cluster. Chen and Houze (1997) suggested that the diurnal cycle of a cloud cluster reflects the life cycle of a larger DC area over the western tropical Pacific. They used three TBB thresholds of 208K, 235K and 260K for cloud cluster identification.

Machado et al. (1998) investigated the life cycle of DCs over America and the eastern Pacific using International Satellite Cloud Climatology Project (ISCCP) B3 data for 1987 and 1988. In their study, they developed an automated method to track convective systems using TBB thresholds of 218 K and 245 K. Their results indicated that convective systems with shorter lifetimes and smaller areas exhibited lower initial expansion rates, lower cloud tops, and lower anvil cloud reflectance than convective systems with longer lifetimes and larger areas.

Mathon and Laurent (2001) studied the life cycle of convective cloud systems over the Sahelian region using the TBB thresholds of 213 K, 233K and 253K. They found that the DC radius was related to its lifetime, as shown by Machado et al. (1998). Further, they found that DC is likely to propagate faster during the mature stage when convection is stronger.

In these studies, the relatively colder TBB thresholds of 235K to 208K have been used for delineating the core of a DC and for inferring the anvil cloud by also using the second and third warmer TBB thresholds. However, there is no physical rationale for delineating an anvil by using the second and third warmer TBB threshold. Further, if we use a colder threshold, we might discard both the beginning (low-level cumulus) and ending (thin anvil cloud) stages of the DC in the life cycle, since the colder threshold can only delineate the deeper parts of the DC.

Inoue (1985) demonstrated the feasibility of cirrus type cloud detection using split window (11 μm and 12 μm) data. Furthermore, a simple method for classifying several cloud types objectively based on a threshold technique applying the two-dimensional diagrams of the TBB and brightness temperature difference (BTD) between the split window was developed (Inoue: 1987, 1989). The 11 μm channel is more transparent than the 12 μm channel for ice. Thus, the TBB at 11 μm is higher than that at 12 μm for an ice cloud. Therefore, the BTD indicates a larger value for a cirrus type cloud consisting of ice, while an optically thick cumulus type cloud exhibits a smaller BTD due to its black-body characteristics. Utilizing these characteristics of the split window, we can classify optically thick cumulus type clouds and optically thinner cirrus type clouds on a more physical basis using a single infrared threshold.

The advent of the Tropical Rainfall Measuring Mission (TRMM) satellite enables us to bridge cloud characteristics and rainfall characteristics over a wide area of the tropics, since the TRMM satellite carries a Precipitation Radar (PR), a microwave radiometer (TRMM Microwave Imager; TMI) and a Visible Infrared Scanner (VIRS) are onboard the TRMM satellite (Kummerow et al., 2000). The PR is the first satellite-borne precipitation radar to observe three-dimensional rainfall structures over a 215 km swath. We can obtain the rainfall rate, sea surface temperature (SST), total precipitable water (TPW) and so on from TMI observation. VIRS has one visible, one near-infrared, and three infrared channels, identical to the visible/infrared sensors on current polar-orbital and geostationary satellites. Temporal sampling is a drawback of the TRMM data in studying the evolution of DCs.

Combining the TRMM and infrared observations from the Japanese Geostationary Meteorological Satellite (GMS), Kondo et al. (2006) investigated the relationship between the evolutionary stage of DCs and rain information. They tracked cloud systems defined by a TBB threshold of 235 K using GMS data for June, July, and August 2000 over the western tropical Pacific. They found that during the lifecycle of the DC the maximum rainfall rate appeared first, then the minimum TBB appeared followed by the maximum area size.

Inoue and Aonashi (2000) examined the relationship between cloud information from the split window of VIRS and the precipitation area from PR. They found that the clouds colder than 260K in TBB with smaller BTD corresponded well to the rain area observed by PR, based on a dataset of rain events during June 1998 over the frontal zone in East Asia. However, they noted some drawbacks of the VIRS calibration. The BTD for a very cold cloud and cumulonimbus type cloud, which can be assumed to be black-body, is larger than that observed by the split window of current polar-orbital satellite and geostationary satellites.

In this study, we aim to investigate the characteristics of DCs and rainfall over the tropical eastern Pacific using TRMM and GOES-W data. The area was selected because of the wide range of SST and the split window on GOES-W was reasonably calibrated. Applying cloud type classification by the split window, we can identify the anvil (cirrus type) clouds within the DC with more physical rationale than through the use of single infrared channel data. We can also monitor a long lasting DC, since cloud type classification by the split window is effective for both day and night. First, we study the life cycle of the DC in terms of cloud type classified by the split window, then we study the characteristics of DC and rainfall using the coincident observations by TRMM and GOES-W.

2. Data

Hourly split window data acquired by GOES-W from January 2001 to December 2002 (excluding September 2001) was used to study the life cycle of DCs. The split window data were gridded to a 0.1-degree latitude/longitude grid over 30N to 30S and 180 to 90W. Clouds were classified at each grid point using the split window. Figure 1 presents the cloud type classification diagram used in this study. We used TBB thresholds of 213K, 235K, 253K, and 263K to classify the optically thick clouds into high, middle, and low levels. Thresholds of 213K and 235K are often used in studies of DCs (e.g., Machado et al., 1998; Mathon and Laurent, 2001) and a 253K threshold corresponding to the temperature at 400hPa in the US tropical standard atmosphere is used as the warmer end of the high-level cloud category.

For BTD thresholds, we used 0.5K and 1K to classify optically thick cloud, and BTD over clear sky to classify the optically thinner cirrus type clouds. The temperature resolution of infrared data at lower TBBs is generally worse than at higher TBBs. Further, we use BTD (BTD=TBB11μm – TBB12μm), which becomes noisy at lower TBBs. Therefore, we used the 1K thresholds to classify the optically thick cloud in this study. Over clear sky areas of the tropics, the BTD indicates about 2K due to differential absorption by water vapor in the atmosphere. Therefore, we used the 2K thresholds to classify the optically thin cirrus type clouds. Here we classified 17 cloud types based on the TBB and BTD as seen in Fig.1, although some cloud types are combined ; these appear in colored ellipses in this study.

We define a DC as a cloud area colder than 253K (cloud types numbers 9 to 17 in Fig.1). Compared to the previous study, the threshold of 253K is on the warmer end for defining a DC. Using a BTD threshold of 1K, we can identify the anvil cloud (an optically thinner area: cloud types 11,12, 15 and 16 in Fig.1) within the DC on a more physical basis than with conventional single infrared channel usage. We also used a cloud lidar (Cloud-Aerosol LIdar with Orthogonal Polarization (CALIOP)) to provide an example of cloud type classification by the split window.

The TRMM is in a non-sun-synchronous orbit with an inclination of 35°. The TRMM PR observes three-dimensional rain structures. Rainfall rate, TPW, and SST are retrieved from TRMM's TMI. 3G68 data was also used in this study. The rainfall information observed by TRMM PR and TMI was assembled on a 0.5-degree latitude/longitude grid.

We compiled information on DCs, such as its size and percentage of cirrus type clouds, extracted using the tracking technique applied to hourly data for the 23 months from January 2001 to December 2002 (no data for September 2001). No-merge and no-split DCs were selected from the tracked DC information for studying the life cycle of a DC. We also selected a DC that coincided with TRMM observations within 15 minutes in order to study the relationship between life stage and rainfall rate.

3. Results

3.1 Cloud type classified by the split window

The classification of cloud types by the split window has been validated in terms of radiative effect by a comparison between coincident and collocated observations from the Earth Radiation Budget Experiment (ERBE) and the cloud types determined by split window (Inoue and Ackerman, 2002). As expected, cirrus type clouds and low-level stratocumulus type clouds classified by the split window exhibit small differences in the values of longwave fluxes, while cirrus type clouds exhibit much smaller values than low-level stratocumulus type clouds in shortwave fluxes. Some of the thin cirrus type cloud classified by the split window indicated positive cloud radiative forcing at the top of the atmosphere. Cloud types other than thin cirrus type clouds classified by the split window indicated significant negative cloud radiative forcing.

Here, we demonstrate an example of the comparison between the cirrus and cumulonimbus type clouds classified by the split window and CALIOP observation. Figure 2 depicts a cloud type classification map constructed from the split window of the Geostationary Operational Environmental Satellite (GOES-10) with Cloud-Aerosol Lidar and Infrared Pathfinder Satellite Observation (CALIPSO) orbit (Fig.2a) over the area of 15S to 25S and 165W to 155W; the data were acquired by GOES-W at 0000 UTC on 30 December, 2006. The backscatter coefficients observed by CALIOP and the cloud types encountered along the orbit (top) are given in Fig.2b. We can see that the cumulonimbus type clouds (cloud types 9, 10, 13, and 14) surrounded by cirrus type clouds (cloud types 4, 8, 12, and 13) over 19S (Fig. 2a). This cloud area corresponds to a complicated vertical cloud structure as seen in Fig. 2b. The cumulonimbus type cloud labeled B corresponds to larger values of the backscatter coefficient. Other cirrus type clouds correspond to relatively smaller values of the backscatter coefficient with the heights greater than 8km seen in Fig.2b. Tiny cirrus type clouds labeled as A, were seen over 15S. This cloud also corresponds to cloud signals higher than 8 km in the CALIOP observations (Fig. 2b). This example indicates the reasonability of cloud type classification by split window for cumulonimbus and cirrus type clouds.

3.2 Evolution of spatial distribution of cloud type associated with DC

Figure 3 shows the two-hourly cloud type distribution maps for the area of 4N to 12N and 157W to 140W from 1200 UTC, 09 May to 0200 UTC, 10 May 2001 (except for 2100 UTC). Time increases from left to right and from top to bottom. The purple area corresponds to clouds colder than 213K (cloud type 17). The blue area corresponds to the cumulonimbus type clouds (cloud types 9,10,13, and 14). This cloud is colder than 253K with BTD smaller than 1K, signifying an optically thicker and colder cloud. The green area corresponds to cirrus type clouds (cloud types 11, 12, 15, and16) that are colder than 253K but optically thinner than a cumulonimbus type cloud.

The DC labeled A in the figure (highlighted by black ellipse) developed until 1600 UTC (top right) with the expansion of a cumulonimbus type cloud and 213K cloud. An anvil cloud area (green) colder than 235K and with BTD larger than 1K then expands with time. The cumulonimbus type cloud had almost disappeared by 2100 UTC on 9 May (middle right). The single infrared channel technique cannot identify differences in optical features within a cloud colder than 253K.

DC labeled B (highlighted by red ellipse) developed very rapidly with a larger area of 213K cloud until 0000 UTC on 10 May (bottom-middle). Thereafter, the 213K cloud decreased and the anvil cloud expanded at 0200 UTC, 10 May (bottom-right). The

DC disappeared at 0700 UTC on 10 May with no cumulonimbus type clouds remaining, just cirrus type clouds (not shown).

We have discussed the life cycle of a DC in terms of cloud type classified by the split window. We see a similar evolution of DCs in many cases (not shown). In the developing stage, cumulonimbus type clouds are dominant, then cirrus type clouds increase with time. The percentage of the cirrus type clouds becomes very large in the decaying stage.

3.3. Temporal variation of cloud amount for each cloud type associated with DC

Figure 4 plots the temporal variations in cloud amount for each cloud type against time from the genesis of the DC labeled A in Fig. 3. The cloud amount peaks with a sequence of clouds colder than 213K, cumulonimbus type cloud, then dense cirrus type clouds colder than 253K with BTD larger than 1K appear. The cloud amount (percentage within the DC) is normalized to the maximum value for each cloud type during the life cycle. Cumulonimbus type clouds or very cold clouds appear in the early stage and cirrus type clouds appear in the later stage of the life cycle. This delineates the DC life cycle characteristics.

We have provided an example of the lifetime of a DC in terms of cloud type.

Such DCs can be tracked using the automated technique developed by Vila et al. (2008). The technique was applied to hourly images captured between January 2001 and December 2002. We selected the DCs that did not split or merge during the lifetime of the DC. The areal center of the DC was assigned as the position of the DC. The number of grids within the DC and the percentage of anvil cloud were archived during the analysis period.

Figure 5a illustrates the temporal variation in the number of grids within the DC (DC size) sorted by the duration of the DC. From the two years, we have 3178 samples for 3 hours duration, 2633 samples for 5 hours duration, 786 samples for 7 hours duration, 262 samples for 9 hours duration, and 132 samples for 11 hours duration. We can see that the DCs with longer lifetime exhibit a larger area (number of grids) at their maximum size. This finding is similar to those of Machado et al. (1998). Machado et al. (1998) suggested that the initial expansion of the DC is a good indicator for the duration of the DC. When we observe the first two time steps in this figure, we can see indications that the initial expansion of the DC is larger for a long lasting DC.

Figure 5b plots the temporal variation in the percentage of cirrus type clouds (anvil) within the DC. Regardless of lifetime, the percentage of cirrus type clouds increases with time. The evolution of cirrus type clouds can be seen in the example in

Figs. 3 and 4. Figure 5c plots the percentage of cirrus type clouds within a DC, using linear interpolation over ten intervals between the initiation time and termination time regardless of the duration of the DC. Although the variance increases toward the end of the lifetime, the percentage of cirrus type clouds increases with time from the initiation of DC.

Thus, the percentage of cirrus type clouds within a DC is a good indicator for determining the life stage (developing, mature, or decaying) of a non-merge or non-splitting DC. In other words, we can, to a large extent, identify the life stage of a DC from a single snapshot satellite image. The percentage of cirrus type clouds in the developing stage is less than 20%, and at the decaying stage it is more than 27%. One might think that this value for the decaying stage seems slightly smaller than expected. However, we note that the end of a DC may not be captured in the hourly data. The actual end of a DC might be a thinner cirrus type cloud that cannot be detected by the 253K threshold.

3.4 DC characteristics and TRMM PR rainfall data

In the previous section, we discussed the DC size and cirrus type percentage during the DC lifecycle for a non-merging or non-splitting DC. We have a general idea that a larger rainfall rate from a DC is associated with the developing or mature stage of the DC lifecycle. Here, we study the relationship between DC characteristics and rainfall information using TRMM PR data. Using the coincident GOES-W and TRMM observation, the closest grid of 3G68 was used for comparisons between DC characteristics and rainfall information. The areal center of the DC was assigned as the position of the DC. Considering the PR observation swath, we selected a DC smaller than 400 grids (about 48,400 km^2).

Figure 6 indicates the rainfall rate (mm/day) from PR for each percentage category of cirrus type cloud within the DC. There was a total of 4434 samples. The rainfall rate is larger for smaller percentages of cirrus type clouds within the DC, which indicates an earlier stage in its lifetime (Fig. 5). The mean rainfall rate becomes very small with a larger percentage of cirrus type clouds within the DC. This suggests that we can qualitatively infer the rainfall rate from a snapshot image by computing the percentage of cirrus type clouds within the DC.

Kondo et al. (2006) demonstrated that the maximum rainfall rate occurs before the maximum size of the DC during its lifetime is reached. The rainfall rate is generally higher in the earlier stage or the mature stage in the DC lifecycle when the DC is smaller. We often see very large cluster where the rainfall rate is low. Thus we believed that there was some relationship between DC size and rainfall rate. Figure 7 indicates the rainfall rate for different numbers of grids (DC size). We cannot see any relationship between DC size and PR rainfall rate (the correlation coefficient is 0.08), although the rainfall rate is slightly higher for 200 to 250 grid category. The smaller DC does not necessarily indicate an earlier stage of its lifetime since the DC is also smaller in the decaying stage, as seen in Fig. 5a.

Therefore, we construct the mean rainfall rate as a function of cirrus type cloud percentage and DC size, using the DCs smaller than 400 grids (about 48,400 km^2). Figure 8 indicates the rainfall rate with shade and contour. The rainfall rate is higher for larger DCs when cirrus type cloud percentage is less than 20%. In contrast, the rainfall rate is generally smaller for both larger DCs and greater percentages of cirrus type clouds within the DC. However, there seems to be a local maximum around a DC size of 200-300 for a cirrus type cloud percentage of 20 to 60%. Because of the narrow swath of TRMM PR, it is difficult to obtain an accurate rainfall rate for a DC larger than 400 grids. If the mature stage of a DC is defined as the maximum rainfall rate during its life cycle, further study is required to determine whether a local maximum of rainfall rate exists in terms of DC size.

4. Concluding Remarks

Generally, DCs (deep convective systems) exhibits complex features in terms of cloud type. It is rare to see a simple evolution from initiation to decay. As seen in Fig. 3, a new deep convection merges with the older convection cell, with deep convection cells appearing one after the other. Some DCs may split into several areas. Through the use of cloud type classification by a split window, we can delineate the anvil cloud (the optically thinner part within the DC) and the core (the optically thicker part) of the DC on a physical basis. In contrast to previous studies that use the TBB threshold to identify DC, our cloud type classification can trace the DC life cycle from the early stages to the later stages of the DC in terms of cloud type.

The lifecycle of a DC in terms of cloud type as classified by the split window was studied over the eastern tropical Pacific (30N to 30S, 180 to 90W). Hourly split window image data from GOES-W for the two years from January 2001 to December 2002 was used in this study. A DC consists mostly of optically thick cumulonimbus type cloud in an earlier stage and increasing cirrus type cloud area increases with time in a later stage. The life stage of DCs can be classified by computing the percentage of cirrus type clouds within the DC. Coincident TRMM PR observation was used to study the relationship between the rainfall rate and the percentage of cirrus type clouds defined by the split window within the DC. As expected, we found that the rainfall rate tends to be higher with a smaller percentage of cirrus type clouds within the DC (during the earlier stages of the life cycle).

Here, we used the hourly data observed from the split window onboard GOES-W. Generally, deep convection is a vigorous phenomenon, with the cloud features changing significantly over time. To capture the features of deep convection, we should use more high frequency observations. Currently Meteosat-8 and 9 observe every 15 minutes, and geostationary satellites planned for the future are also expected to observe with higher frequency. Therefore, further study using these high frequency observations will provide us with another perspective on DCs.

Acknowledgments

This study was supported in part by the TRMM program of the Japan Aerospace Exploration Agency (JAXA) and by the program of Core Research for Evolutional Science and Technology (CREST) under the Japan Science and Technology Agency (JST).

References

Byers, H., and R. Braham Jr., 1949: The thunderstorm, U.S. Weather Bureau.

Chen, S. S. and R. A. Houze, 1997: Diurnal variation and life-cycle of deep convective systems over the tropical Pacific warm pool. Quart. J. Roy. Meteor. Soc., 123, 357-388.

Duvel, J. P., 1989: Convection over tropical Africa and the the Atlantic Ocean during northern summer. Part I: Interannual and diurnal variations. Mon. Wea. Rev., 117, 2782-2799.

Inoue, T., 1985: On the temperature and effective emissivity determination of semi-transparent cirrus clouds by bi-spectral measurements in the 10 μm window region. J. Meteor. Soc. Japan., 63, 88-99

Inoue, T., 1987: A cloud type classification with NOAA-7 split window measurements. J. Geophys. Res., 92, 3991-4000

Inoue, T., 1989: Features of clouds over the tropical Pacific during northern hemisphere winter derived from split window measurements. J. Meteor. Soc. Japan., 67, 621-637.

Inoue, T and K. Aonashi, 2000: A comparison of cloud and rainfall information from instantaneous visible and infrared scanner and precipitation radar observations over a frontal zone in east Asia during June 1998. J. Appl. Meteor., 39, 2292-2301

Inoue, T. and S. Ackerman, 2002: Radiative effect of various cloud types as classified by the split window technique over the eastern sub-tropical Pacific derived from collocated ERBE and AVHRR data. J. Meteor. Soc. Japan, 80, 1383-1394.

Kondo, Y. A. Higuchi and K. Nakamura, 2006: Small-scale cloud activity over the maritime continent and the western Pacific as revealed by satellite data. Mon. Wea. Rev., 134, 1581- 1599.

Kummerow, C., et al., 2000: The status of the tropical rainfall measuring mission

(TRMM) after two years in orbit, *J. Appl. Meteor.*, 39, 1965-1982.

Machado, L. W. Rossow, R. Guedes and A Walker, 1998: Life cycle variations of mesoscale convective systems over the Americas. Mon. Wea. Rev., 126, 1630-1654

Mapes B., and R. A. Houze, 1993: Cloud cluster and superclusters over the oceanic warm pool. Mon. Wea. Rev., 121, 1398-1415.

Mathon, V. and H. Laurent, 2001: Life cycle of the Sahelian mesoscale convective systems. Quart. J. Roy. Meteor. Soc., 127, 377-406.

Murakami, M. ,1983: Analysis of deep convective activity over the western Pacific and south east Asia. Part I: Diurnal variation. J. Meteor. Soc. Japan, 61, 60-75.

Nakazawa, T., Tropical supper cluster within intraseasonal variations over the western Pacific. J. Meteor. Soc. Japan, 66, 823-839.

Takayabu, Y. N., 1994: Large-Scale Cloud Disturbances Associated with Equatorial Waves. Part I: Spectral Features of the Cloud Disturbances. J. Meteor. Soc. Japan, 72, 433-449

Vila, D.A., L.A.T. Machado, H. Laurent, and I. Velasco, 2008: Forecast and Tracking the Evolution of Cloud Clusters (ForTraCC) Using Satellite Infrared Imagery: Methodology and Validation. Wea. Forecasting, 23, 233–245.

Wentz, F. J. and T. Missner, 2000: AMSR Ocean Algorithm: ATBD Version 2. NASA Reference Publication, 66 pp.

Williams, M. and R. A. Houze, 1987: Satellite-observed characteristics of winter monsoon cloud cluster. Mon. Wea. Rev., 115, 505-519.

Figure Captions

Fig. 1 Cloud type classification diagram using the split window data. Cumulonimbus type clouds (colder TBB with small BTD) are indicated by numbers 9,10,13, and 14 (blue ellipse) as well as 17 (purple ellipse). Dense cirrus type clouds (colder TBB with larger BTD) are indicated by numbers 11,12,15, and 16 (green ellipse). Cirrus type clouds (warmer TBB with larger BTD) are indicated by numbers 4 and 8 (light green ellipse). Low-level cumulus type cloud (warmer TBB with small BTD) are indicated by numbers 1, 2, 5, and 6.

Fig. 2a Cloud type map (cumulonimbus type clouds in blue color and cirrus type clouds in green) as classified by the split window over 15S to 25S and 165W to 145W at 0000 UTC on 30 December 2006 with CALIPSO orbit (yellow line).

Clouds labeled A and B along the CALIPSO orbit correspond to A and B in Fig. 2b.

Fig. 2b Vertical profile of backscatter coefficient observed by CALIOP over 15S to 25S along the CALIPSO orbit in Fig.2a Corresponding cloud types are shown on top with the same colors as in Fig.2a.

Fig. 3 Two hourly cloud type maps for the case of deep convective activity from 09 May to 10 May, 2001. Time increases from left to right and from top to bottom.

Fig. 4 Temporal variations in cloud amount within DC for each cloud type during the life cycle for the DC called A in Fig 3. The cloud amount is normalized to the maximum value for each cloud type. CB, DCI and 213K denote the respective cumulonimbus type cloud (cloud types 9,10,13, and 14 in Fig.1), dense cirrus type clouds (cloud types 11,12,14, and 15) and clouds colder than 213K (cloud type number 17 in Fig. 1), respectively.

Fig. 5a. Evolution of DC size (number of 0.1-degree latitude/longitude grids) sorted by duration of lifetime

Fig. 5b. Evolution of the percentage of cirrus type clouds within a DC, sorted by duration of lifetime

Fig. 5c Evolution of the percentage of cirrus type clouds, normalized to the lifecycle. The middle line indicates the mean and other lines indicate the offset of the standard deviation from the mean value.

Fig. 6 Rainfall rate (mm/day) from TRMM PR and the percentage of cirrus type clouds within the DC. The bold bars and box indicate the respective median value in each category and the first and third quartile.

Fig. 7 Mean rainfall rate (mm/day) from TRMM PR, and DC size (number of 0.1-degree latitude/longitude grids). Bars indicate standard errors.

Fig.8 Mean rainfall rate indicated with both shade and contour as a function of the cirrus type cloud percentage and DC size

Fig. 1

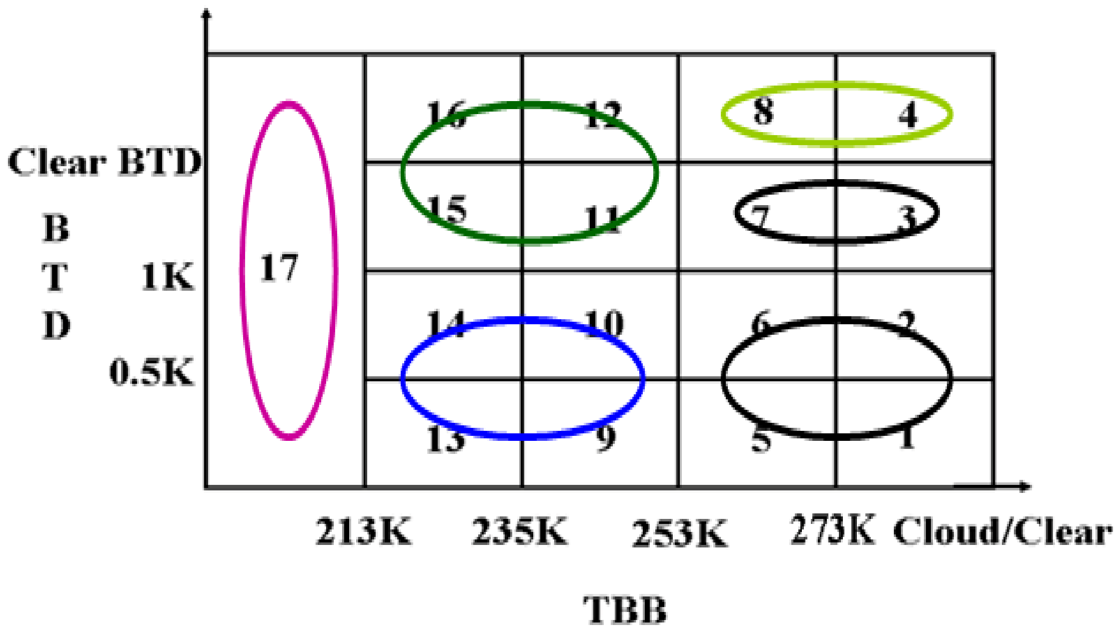
Clear BTD
B
T
D
1K
0.5K
17
16
12
15
11
14
10
13
9
8
4
7
3
6
2
5
1
213K
235K
253K
273K
Cloud/Clear
TBB

Fig. 2a

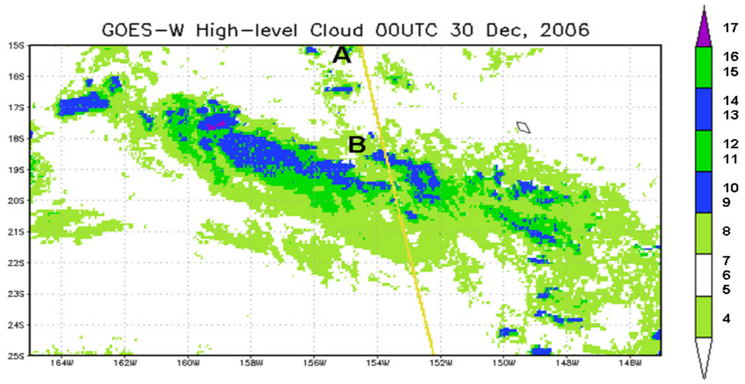
GOES-W High-level Cloud 00UTC 30 Dec, 2006
A
B
15S
16S
17S
18S
19S
20S
21S
22S
23S
24S
25S
164W
162W
160W
158W
156W
154W
152W
150W
148W
146W
17
16
15
14
13
12
11
10
9
8
7
6
5
4

Fig. 2b

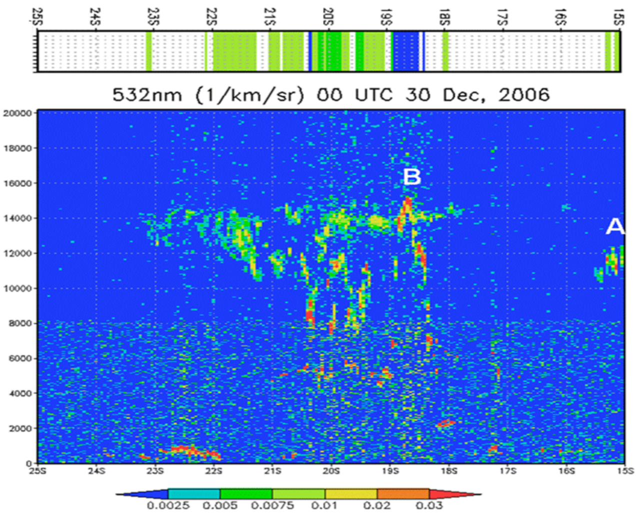
25S
24S
23S
22S
21S
20S
19S
18S
17S
16S
15S
532nm (1/km/sr) 00 UTC 30 Dec, 2006
B
A
20000
18000
16000
14000
12000
10000
8000
6000
4000
2000
0
0.0025
0.005
0.0075
0.01
0.02
0.03

Fig. 3

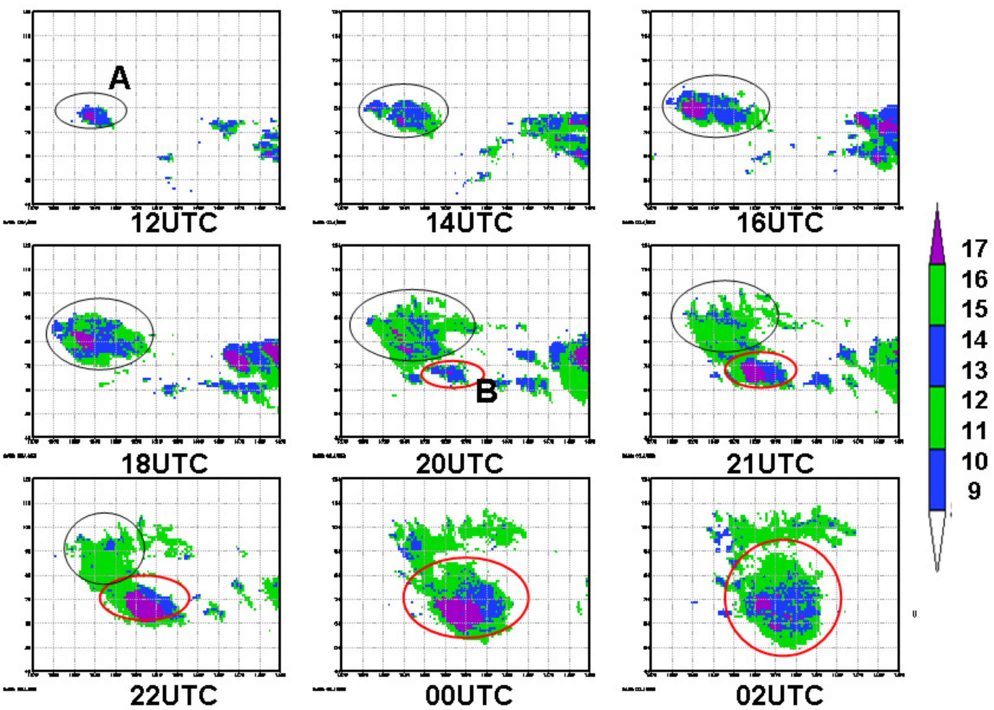
A
12UTC
14UTC
16UTC
18UTC
B
20UTC
21UTC
22UTC
00UTC
02UTC
17
16
15
14
13
12
11
10
9

Fig. 4

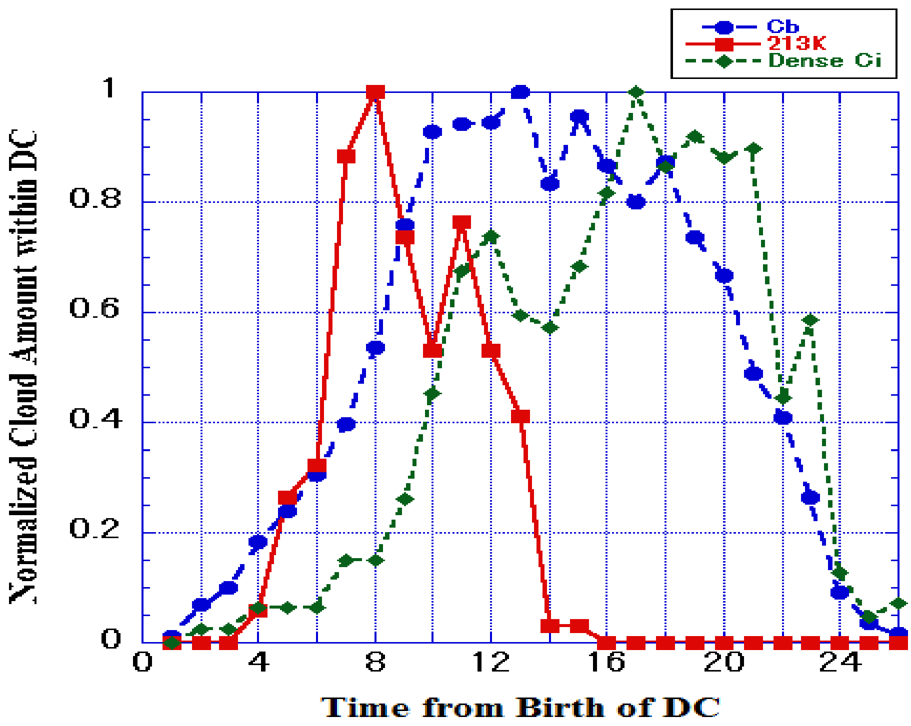
Cb
213K
Dense Ci
Normalized Cloud Amount within DC
Time from Birth of DC
0
0.2
0.4
0.6
0.8
1
0
4
8
12
16
20
24

Fig. 5a

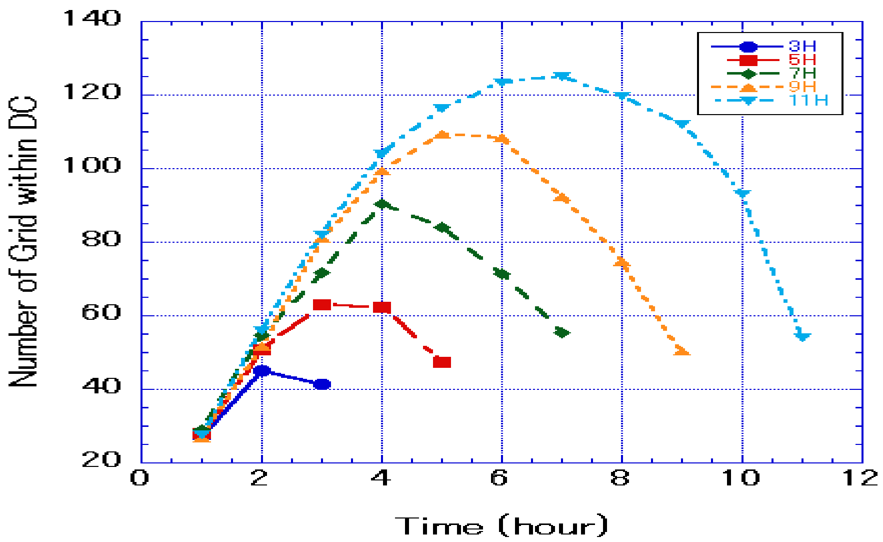
3H
5H
7H
9H
11H
Number of Grid within DC
Time (hour)
140
120
100
80
60
40
20
0
2
4
6
8
10
12

Fig. 5b

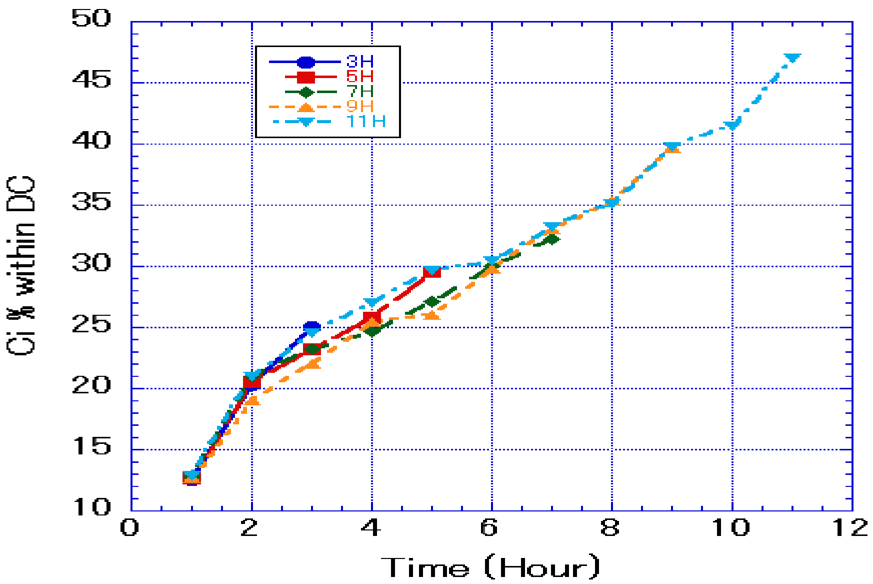
3H
5H
7H
9H
11H
Ci % within DC
Time (Hour)
50
45
40
35
30
25
20
15
10
0
2
4
6
8
10
12

Fig. 5c

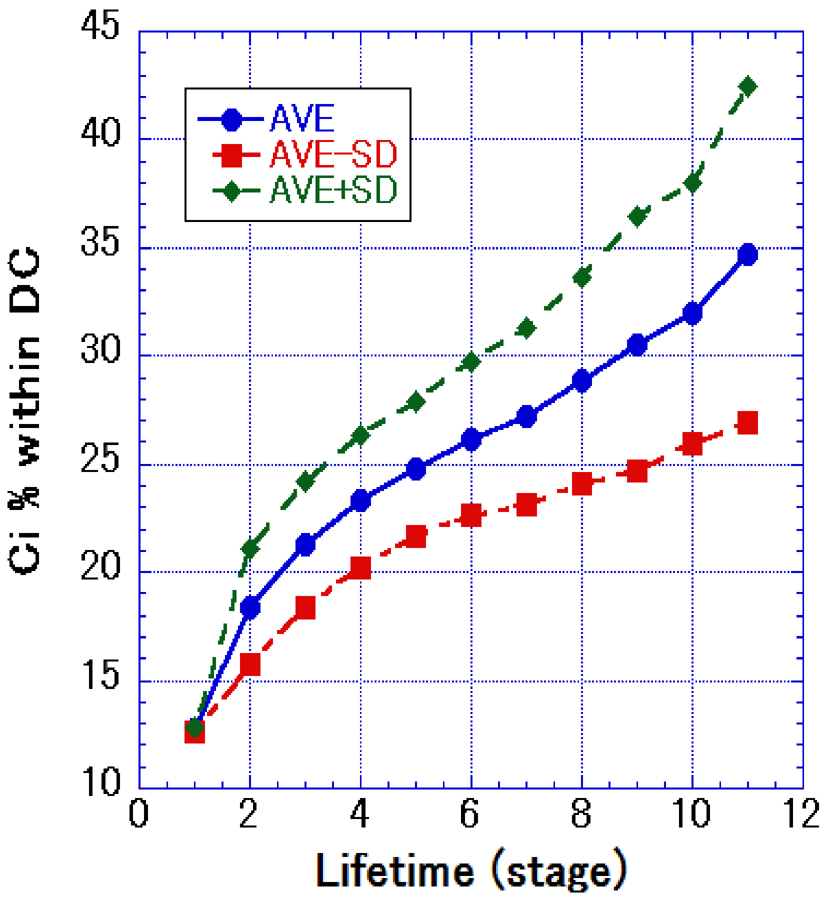
AVE
AVE−SD
AVE+SD
Ci % within DC
Lifetime (stage)
45
40
35
30
25
20
15
10
0
2
4
6
8
10
12

Fig. 6

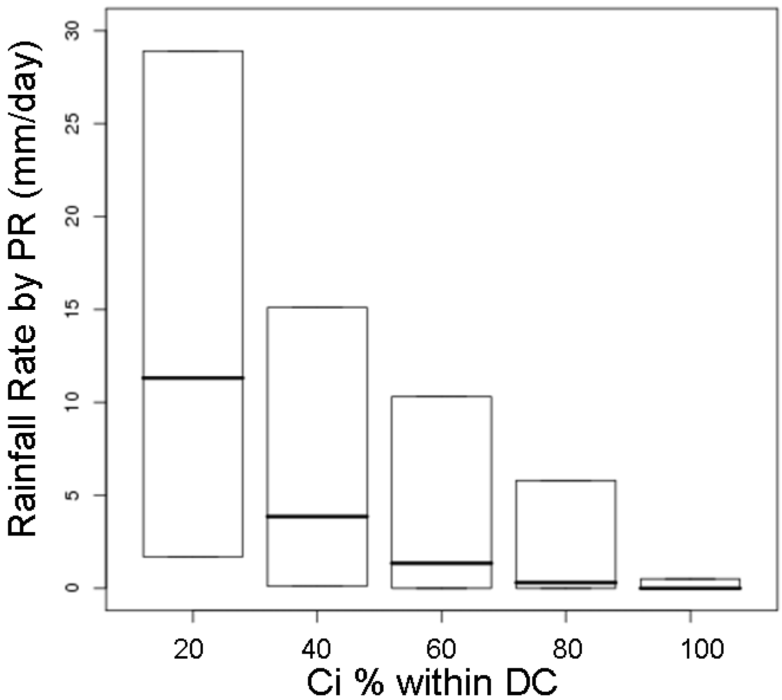
Rainfall Rate by PR (mm/day)
0
5
10
15
20
25
30
20
40
60
80
100
Ci % within DC

Fig. 7

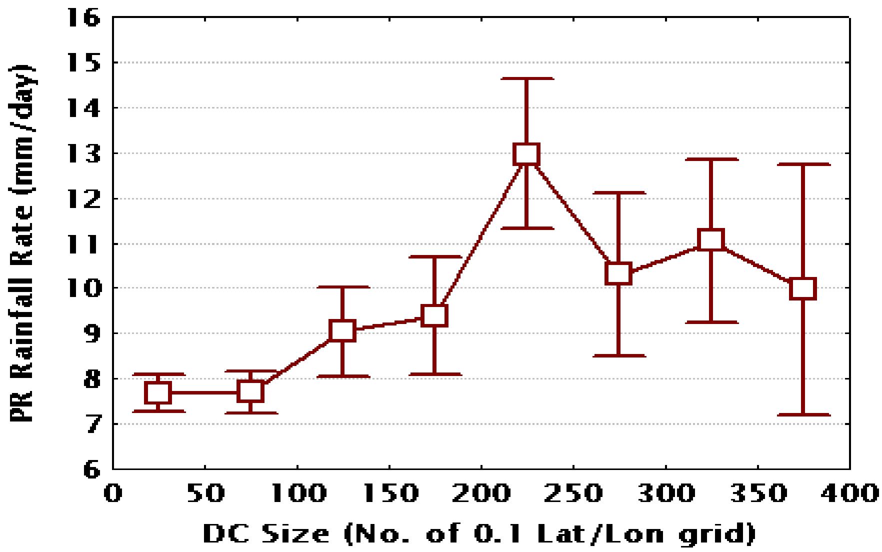
PR Rainfall Rate (mm/day)
16
15
14
13
12
11
10
9
8
7
6
0
50
100
150
200
250
300
350
400
DC Size (No. of 0.1 Lat/Lon grid)

Fig. 8

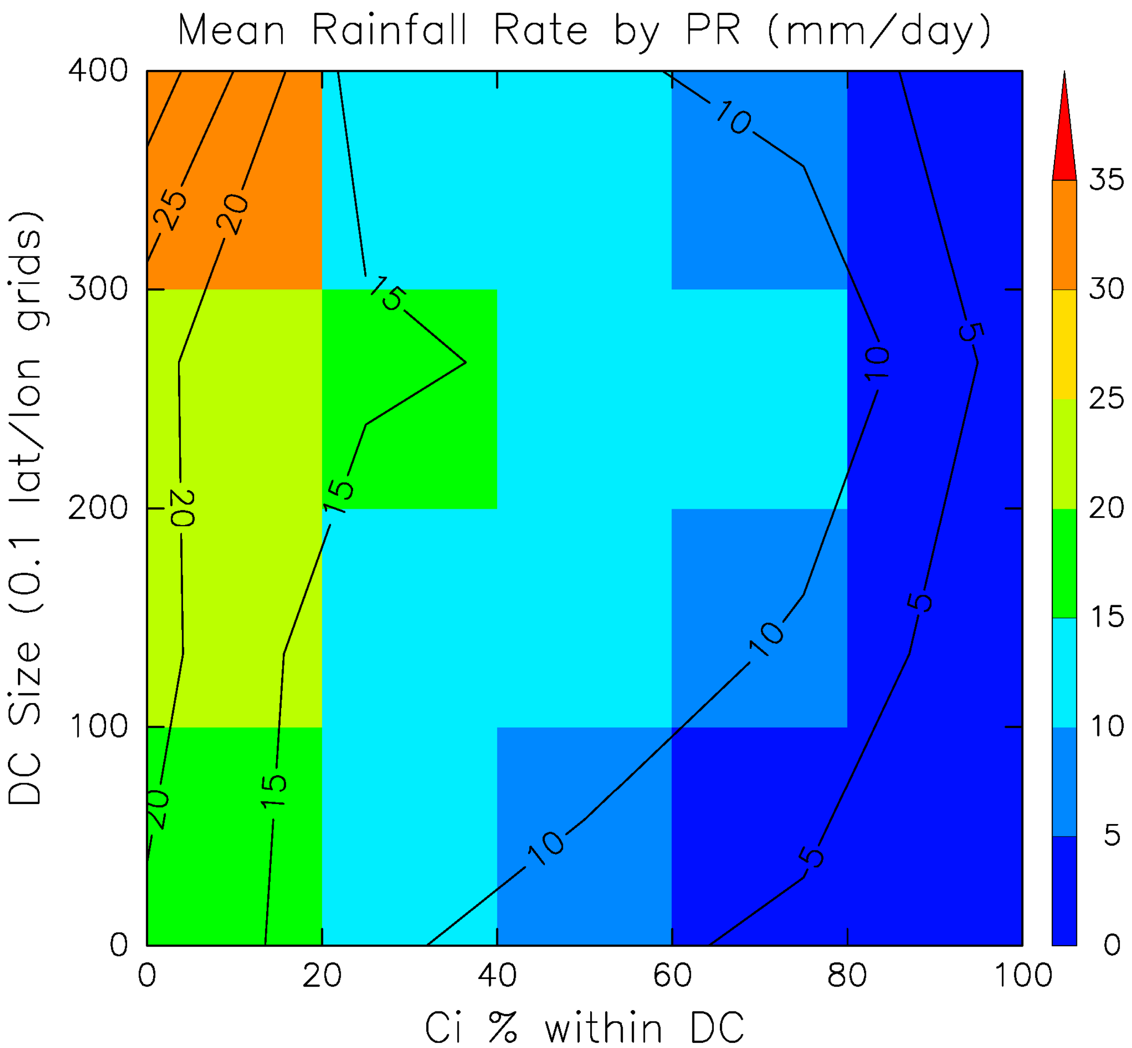
Mean Rainfall Rate by PR (mm/day)
DC Size (0.1 lat/lon grids)
Ci % within DC
0
100
200
300
400
0
20
40
60
80
100
0
5
10
15
20
25
30
35